ADVANCES IN ATMOSPHERIC SCIENCES, VOL. 30, NO. 1, 2013, 101–115

Effect of Boundary Layer Latent Heating on MJO Simulations

LING Jian*[1] (凌 健), LI Chongyin[2] (李崇银), ZHOU Wen[3] (周 文),
JIA Xiaolong[4] (贾小龙), and Chidong ZHANG[1]

[1] *Rosenstiel School of Marine and Atmospheric Science, University of Miami, Miami, Florida* 33149

[2] *The State Key Laboratory of Numerical Modelling for Atmospheric Sciences and Geophysical Fluid Dynamics, Institute of Atmospheric Physics, Chinese Academy of Sciences, Beijing* 100029

[3] *Guy Carpenter Asia-Pacific Climate Impact Centre, School of Energy and Environment, City University of Hong Kong, Hong Kong*

[4] *Climate Prediction Division, National Climate Center, Beijing* 100081

(Received 12 February 2012; revised 26 March 2012)

ABSTRACT

A latent heating peak in the PBL was detected in a simulation by a global GCM that failed to reproduce Madden–Julian Oscillation (MJO). The latent heating peak in the PBL was generated by very shallow convection, which prevented moisture from being transported to the free troposphere. Large amount of moisture was therefore confined to the PBL, leading to a dry bias in the free atmosphere. Suffering from this dry bias, deep convection became lethargic, and MJO signals failed to occur. When the latent heating peak in the PBL was removed in another simulation, reasonable MJO signals, including the eastward propagation and the structure of its large-scale circulation, appeared. We therefore propose that the excessive latent heating peak in the PBL due to hyperactive shallow convection may be a reason for a lack of MJO signals in some simulations by other GCMs as well.

Key words: Madden–Julian Oscillation (MJO), latent heating, planetary boundary layer (PBL)

Citation: Ling, J., C. Y. Li, W. Zhou, X. L. Jia, and C. D. Zhang, 2013: Effect of boundary layer latent heating on MJO simulations. *Adv. Atmos. Sci.*, **30**(1), 101–115, doi: 10.1007/s00376-012-2031-x.

1. Introduction

Madden–Julian Oscillation (MJO, Madden and Julian, 1971, 1972) is an important phenomenon in the tropical atmospheric weather and climate systems (Madden and Julian, 1994; Lau and Waliser, 2005; Zhang, 2005). Accurate simulation of MJO can yield tremendous benefits to numerical weather prediction. However, most state-of-the-art atmospheric general circulation models (AGCMs) fail to reproduce the most salient features of the MJO, such as its slow eastward propagating speed (Slingo et al., 1996; Lin et al., 2006; Kim et al., 2009). Cumulus parameterization has been identified as the key factor that determines whether the MJO can be well simulated (e.g., Wang and Schlesinger, 1999; Maloney and Hartmann, 2001; Rajendran et al., 2002; Lee et al., 2003; Liu et al., 2005; Jia et al., 2010). Such influences of cumulus parameterization on MJO simulations were well demonstrated (Fig. 1). An AGCM [SAMIL, Spectral Atmosphere Model of State Key Laboratory of Numerical Modeling for Atmospheric Sciences and Geophysical Fluid Dynamics (LASG) in the Institute of Atmospheric Physics (IAP)] with a moist convection adjustment (MCA) scheme (Manabe and Strickler, 1964) could well simulate the eastward propagating characteristics of the MJO (Fig. 1a), albeit with faster propagating speed ($\sim$8 m s^{-1}), whereas it failed when the cumulus parameterization was changed to the Tiedtke (1989) scheme (Fig. 1b). In AGCMs of coarse resolution, cumulus parameterization schemes are crucial in determining the dominant part of precipitation in

*Corresponding author: LING Jian, jling@rsmas.miami.edu

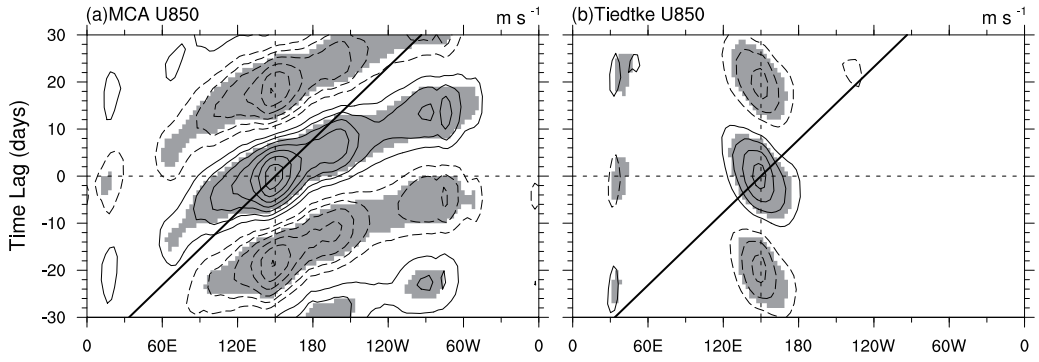

Fig. 1. Lag regression of MJO band (time periods of 30–90 days and zonal wavenumbers 1–5) filtered zonal wind at 850 hPa (interval: 0.2 m s^{-1}) averaged over 15°S–15°N on the reference point at 150°E from SAMIL with (a) the MCA scheme and (b) the Tiedtke scheme. Dashed contours for negative values and zero contours were omitted. Results passing significance test with the 90% confidence level or above are shaded. The bold solid lines stand for the 5 m s^{-1} eastward propagation speed.

the tropical region. Convective momentum transport (CMT) may also affect MJO simulations (e.g., Zhang and McFarlane, 1995; Gregory et al., 1997; Inness and Gregory, 1997; Ling et al., 2009). CMT was not included in this study because it is not represented by either the MCA or Tiedtke schemes used in the simulations.

Interaction between latent heating released by condensation and large-scale circulation has been considered the key process in MJO theories emphasizing moisture convergence (Wang and Rui, 1990; Wang, 2005) and scale interaction (Majda and Stechmann, 2009). Some studies have indicated that the slow eastward-propagating speed of MJO is related to shallow convective heating (Li, 1985; Lau and Peng, 1987; Takahashi, 1987; Chang and Lim, 1988; Sui and Lau, 1989), because low-level heating is more effective in promoting higher-order vertical modes with slower phase speeds. Modeling studies have also shown that more organized low-level heating may lead to more robust MJO signals in numerical simulations (e.g., Zhang and Mu, 2005; Benedict and Randall, 2007; Li et al., 2009; Zhang and Song, 2009). However, others have suggested that upper-level stratiform heating is of primary importance to tropical large-scale circulation (Hartmann et al., 1984; Houze, 1997; Schumacher et al., 2004) and variability (Cho and Pendlebury, 1997; Mapes, 2000) in general and to MJO (Fu and Wang, 2009) in particular.

The role of latent heating in MJO dynamics has also been suggested by observations, but not without controversy. Sounding observations from the Tropical Ocean Global Atmosphere Coupled Ocean-Atmosphere Response Experiment (TOGA-COARE, November 1992 to February 1993, Webster and Lukas, 1992) reveal that the preceding low-level shallow convective heating and the successive trailing stratiform-like upper-level heating constitute a westward tilt in diabatic heating are associated with eastward-propagating MJO (Lin et al., 2004; Kiladis et al., 2005). However, such westward tilt is not evident in recent sounding observations over the central equatorial Indian Ocean during the Mirai Indian Ocean Cruise for the Study of the MJO-Convection Onset (MISMO, Katsumata et al., 2009). Recent studies have demonstrated that the evolution of heating profiles associated with the MJO may not be the same at different logitudinal locations for a given MJO event or for different MJO events at the same location (Zhang et al., 2010; Ling and Zhang, 2011).

Latent heating profiles from two simulations by an AGCM (SAMIL, see section 2.1) both show largely the same bottom-heavy distribution, with a peak nearly at 500–700 hPa above the PBL (Fig. 2, dotted lines). The distinct difference between the two is in the PBL. The one with a significant latent heating peak in the PBL (cyan dotted line) was produced using the Tiedtke scheme that failed to reproduce the eastward propagation of MJO (Fig. 1b). The latent heating peak in the PBL is absent in the other (blue dotted line) which was produced by the MCA scheme that led to reasonable MJO simulation (Fig. 1a). A distinct peak of latent heating in the PBL can also be found in global reanalysis data and in other AGCMs, such as the Community Atmosphere Model version 3 (CAM3) and the Tropical channeled Weather Research and Forecast (TWRF) model (Fig. 2, yellow and red lines); neither have been able to simulate the eastward propagation of MJO. Latent heating from two recent global reanalysis data sets, the Climate Forecast System Reanalysis (CFSR,

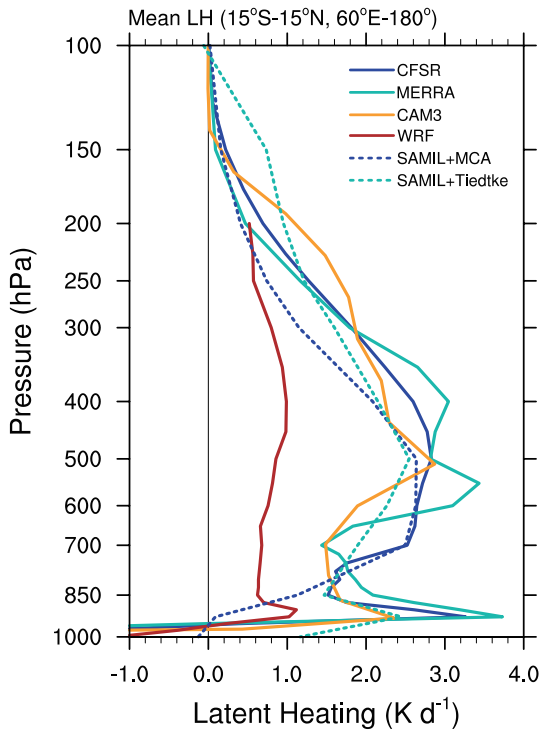

Fig. 2. Mean latent heating profiles averaged over 15°S–15°N, 60°–180°E from reanalysis data (CFSR and MERRA) and four model simulations (CAM3, WRF, SAMIL+MAC, and SAMIL+Tiedke).

Saha et al., 2010) and the Modern Era Retrospective Analysis for Research and Applications (MERRA, Bosilovich et al., 2006), have obvious latent heating peaks in the PBL (Ling and Zhang, 2011). However, free runs of the atmospheric models used for data assimilation of these two reanalysis datasets (CFSR and MERRA) have not been able to reproduce MJO characteristics well (see results of CFS and GEOS5 in Kim et al., 2009). The CAM3, WRF, SAMIL with the Tiedtke scheme, and the atmospheric components of two latest reanalysis data assimilation systems have all failed to simulate MJO, and they all have latent heating peaks in the PBL.

The objective of this study was to explore whether the latent heating peak in the PBL is a reason for the absence of MJO signals in AGCMs. Following the approach of Li et al. (2009), numerical experiments were conducted in which latent heating within the PBL in an AGCM was alternated and the corresponding changes in the simulated MJO were examined. The model, the design of the experiments, and the data used in this study are described in section 2. Results are presented in section 3. A summary and discussion are given in section 4.

2. Model and methodology

2.1 *Model*

The AGCM used in this study is a spectral model (referred to as SAMIL) originated by Simmonds (1985) and then developed at the LASG in the IAP of the Chinese Academic of Science (CAS). It is one of the atmospheric components of the Flexible Global Ocean–Atmosphere–Land System model (FGOALS) participating in Intergovernmental Panel on Climate Change Fourth Assessment Report (IPCC AR4) and used frequently in climate study (i.e., Jia et al., 2008; Li et al., 2009; Jia et al., 2010; Wang et al., 2012). The horizontal resolution used in this study is a rhomboidal truncation with maximum wavenumber 42 [R42, 128 ×108 Gaussian grid points, ∼2.8125° (lon.) ×1.66° (lat.)]. A hybrid vertical coordinate is used with 26 atmospheric layers extending from the surface to 2.19 hPa. The parameterization package includes the Edwards and Slingo (1996) scheme for radiation, the Slingo (1980, 1987) scheme for cloud diagnosis, and the Holtslag and Boville (1993) scheme for the boundary layer. A semi-implicit scheme with a time step of 15 minutes is used for integration. Further details of SAMIL are available in Wu et al. (1996).

2.2 *Cumulus parameterization scheme*

The Tiedtke (1989) scheme was used in the sensitivity simulations. It was first implemented in SAMIL by Song (2005). It is a mass flux convection scheme, which can represent shallow, deep, and midlevel convections. However, only one type of convection is allowed to take place each time step at a grid when the scheme is activated. An ensemble of clouds occurring in each type of convection is assumed to consist of updrafts and downdrafts. Mid-level convection mainly occurs in rain bands at warm fronts and in the warm sector of extratropical cyclones and with its root above the PBL. Deep convection mostly occurs when there is a deep layer of conditional instability and larger-scale moisture convergence. Shallow convection mostly occurs in an undisturbed flow (i.e., in the absence of large-scale convergence flow), such as trade wind cumuli under a subsidence inversion. The depth of shallow convective clouds (pressure difference between cloud bottom and top) was less than 200 hPa. The observed deep and shallow convection similar to the first two leading modes in Zhang and Hagos (2009) were both simulated by the deep convection process in this scheme. The latent heating peak in the PBL in this model (discussed in section 1) was generated by shallow convection processes. The details of Tiedtke scheme are available in Tiedtke (1989) and Nordeng (1994). A large-scale adjustment of moist stability and

moisture saturation was applied after this scheme was called at each grid point.

2.3 *Experiment and analysis*

A control run and two sensitive simulations were designed to explore the impact of the latent heating peak in the PBL on MJO simulations. Mid-level convection seldom occurs in the tropical region, and it was left unchanged in this study. In one simulation, latent heating generated by shallow convection was set to zero at each time step; this simulation is referred to as the no shallow latent heating run, or the NSLH run. It was doubled in the second simulation; this simulation is referred to as the double shallow latent heating run, or the DSLH run. Only latent heating from shallow convection was changed in the experiment, while other properties of shallow convection (e.g. cloud top, cloud base, radiative heating) remained intact. Precipitation generated by the shallow convection also remained unchanged. Total latent heating, therefore, did not match precipitation in the NSLH and the DSLH runs at the grid point where the shallow convection occurred (discussed in section 3.1). This mismatch between precipitation and latent heating should not cause concern, because the water vapor source over the ocean, where most shallow convection in the model occurred (see Fig. 3a), did not depend on precipitation. The first sensitive experiment was designed to verify the effect of the existence of the latent heating peak in the PBL on the MJO simulation, and the second simulation was designed to verify the influence of its amplitude. All simulations were run for 11 years. Initial conditions were based on NCAR/NCEP reanalysis data (Kalnay et al., 1996). Climatology monthly mean SST and sea ice were used as the surface conditions. The last 10 years of the simulations were used to diagnose MJO signals.

The main diagnostic variables included zonal wind, vertical velocity, latent heating, and specific humidity (q). The MERRA (Bosilovich et al., 2006) product was used to validate the model outputs.

The variable, EPR, derived from latent heating, was later used instead of precipitation as a regression index. It has a linear relationship to vertically integrated latent heating. Its value represents the amount of the precipitation generated by a specific latent heating profile.

$$\mathrm{EPR} = \frac{c_p}{gL_c\rho_l}\sum_{i=1}^{n}\left(\Delta p_i H_i\right), \tag{1}$$

where c_p is the specific heat capacity of dry air, i is the index for vertical levels, ρ_i is the density, Δp_i is the pressure depth, H_i is the latent heating tendency at level i, L_c is the latent heat of condensation at 0°C, ρ_l is the density of liquid water, and n is the total number of vertical levels in the troposphere.

The large-scale moisture budget was used to evaluate the vertical moisture transport using the subgrid process parameterized in the convective scheme according to the method of Yanai et al. (1973):

$$-\left(\frac{\partial\bar{q}}{\partial t}+\frac{\partial\bar{u}\bar{q}}{\partial x}+\frac{\partial\bar{v}\bar{q}}{\partial y}+\frac{\partial\bar{\omega}\bar{q}}{\partial p}\right)=\frac{\partial}{\partial p}\left(\overline{q'\omega'}\right)+(c-e)\ , \tag{2}$$

where q is specific humidity, (u, v, ω) is the three-dimensional wind in pressure coordinates, and c/e is the rate of condensation/evaporation per unit mass of air, which is directly related to latent heating in the AGCM. Deviations from the horizontal averages, or perturbations in the subgrid are denoted by primes, while horizontal averages are denoted by bars. The first term on the right side of Eq. (2) is the vertical moisture transport by eddy flux, which is dominated by subgrid-scale convection. After the long-term mean is applied to Eq. (2), the first term on the left side ($\partial\bar{q}/\partial t$) can be ignored and the long-term mean budget equation can be written as follows:

$$\left[\frac{Hc_p}{L_c}\right]=-\left[\frac{\partial}{\partial p}\left(\overline{q'\omega'}\right)\right]-\left[\frac{\partial\bar{u}\bar{q}}{\partial x}+\frac{\partial\bar{v}\bar{q}}{\partial y}\right]-\left[\frac{\partial\bar{\omega}\bar{q}}{\partial p}\right]\ , \tag{3}$$

where H is latent heating, and [ ] indicates the long-term mean. The term on the left side represents the moisture tendency due to the total contribution of the precipitation and evaporation. The second and third terms on the right side represent the moisture tendency due to larger scale horizontal and vertical convergence or divergence, respectively. The first term on the right side represents the moisture tendency caused by the convection itself. This value cannot be directly calculated, so it was estimated as the residual of Eq. (3).

Anomalous time series were first calculated by removing the annual cycle from the original daily data averaged over 15°N–15°S. MJO filters (time periods of 30–90 days and zonal wavenumbers of 1–5) were then applied to obtain the intraseasoanl anomalies following the method of Kiladis et al. (2009).

3. Results

3.1 *Mean state*

Total latent heating from the control run (Fig. 3a) shows large values in the major convection centers, such as the tropical eastern Indian Ocean–Maritime Continent–western Pacific Ocean, South America, and Africa. The peaks of latent heating over these convection centers occur at 500 hPa, and there is a weak gap over the Maritime Continent. These features are alm-

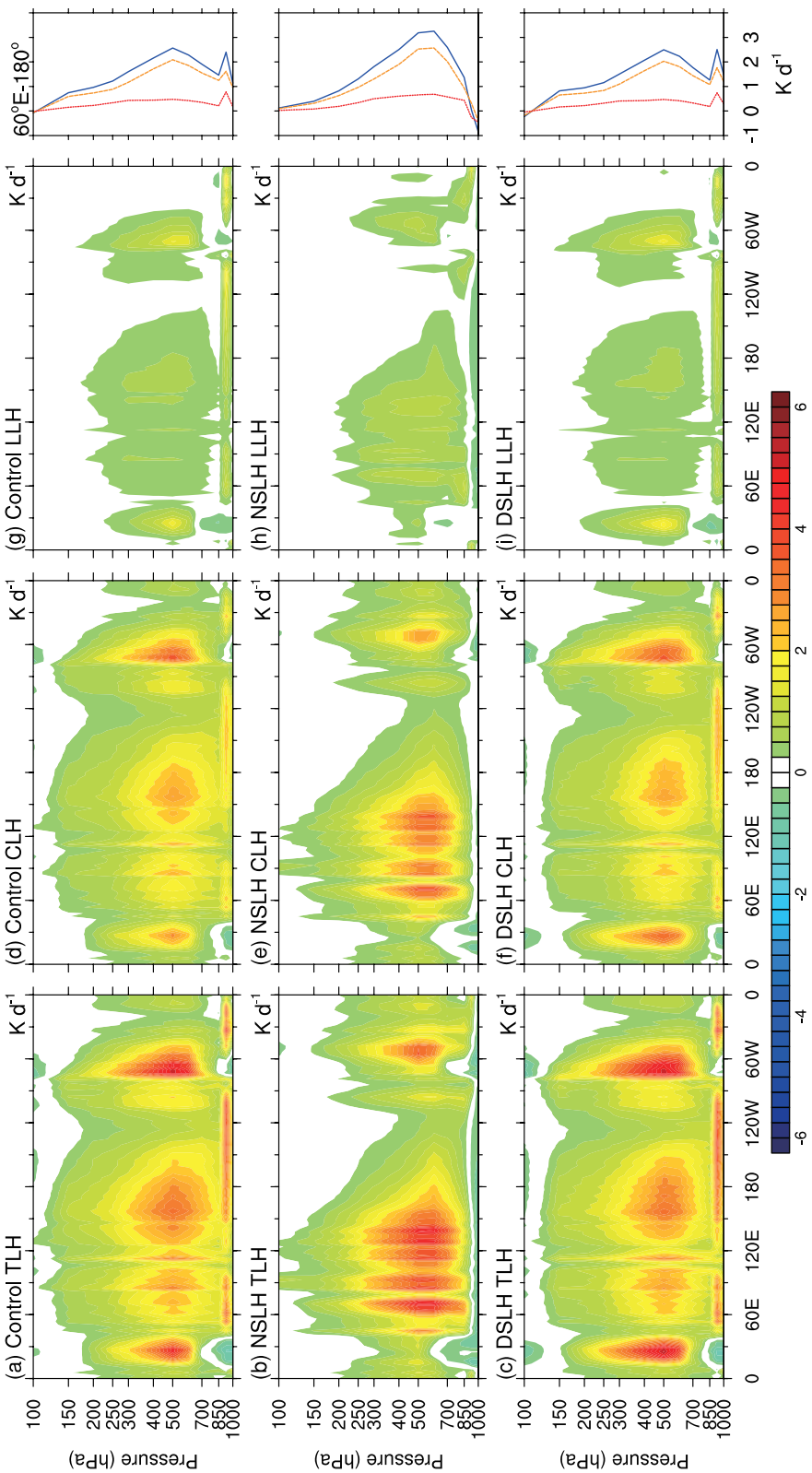

Fig. 3. Longitude–pressure distribution of mean (a–c) total latent heating (TLH, K d^{-1}), (d–f) convective latent heating (CLH, K d^{-1}) , (g–i) large-scale condensation latent heating (LLH, mm d^{-1}), and their mean profiles (solid blue for TLH, dashed orange for CLH, and dotted red for LLH) over 60°–180°E (right panels) from the control run (top panels), the no shallow latent heating run (NSLH, middle), and the double shallow latent heating run (DSLH, bottom). All are averaged over 15°S–15°N.

ost the same as those from Tropical Rainfall Measuring Mission (TRMM) retrievals and reanalyses from previous studies (Zhang et al., 2010; Ling and Zhang, 2011, 2012), albeit with weaker latent heating over the Indian Ocean. There was a distinct latent heating peak in the PBL in the control run, which only occurred over the ocean, presumably originating from precipitating shallow convection. It disappeared in the NSLH run (Fig. 3b) due to the removal of latent heating from shallow convection. In addition to this, the most distinct difference between the control run and the NSLH run, convection over the eastern Pacific Ocean and Americas became weaker and almost disappeared over Africa in the NSLH run. In contrast, convection over the Indian Ocean, the Maritime Continent, and the western Pacific was enhanced. These are the regions where the MJO exists. Latent heating in the DSLH run (Fig. 3c) changed in convective strength in the opposite direction: latent heating above the PBL was weaker over the eastern Indian Ocean, the Maritime Continent, and the western Pacific, but stronger over the Americas and Africa. Latent heating from convection (Figs. 3d–f) was much larger than from large-scale condensation due to the large-scale adjustment (Figs. 3g–i) in these three simulations. When the latent heating peak in the PBL generated by the shallow convection was removed, latent heating due to large-scale condensation in the PBL became slightly stronger (Fig. 3h). The total amount of change in latent heating from the larger-scale condensation was negligible compared to latent heating from convection. Latent heating from the cumulus parameterization was the dominant component of total latent heating in tropical region in the model. Only total latent heating was examined in the remainder of the study.

The horizontal distribution of the mean state of precipitation and EPR are shown in Fig. 4. Mean precipitation from the control run shows a distinct double ITCZ over the eastern tropical Pacific and Indian Ocean, which was more severe than in most other AGCMs. In comparison, precipitation in the NSLH run was enhanced in the Northern Hemisphere, especially over the Arabian Sea and the Bay of Bengal. Meanwhile, precipitation became weaker in the South-

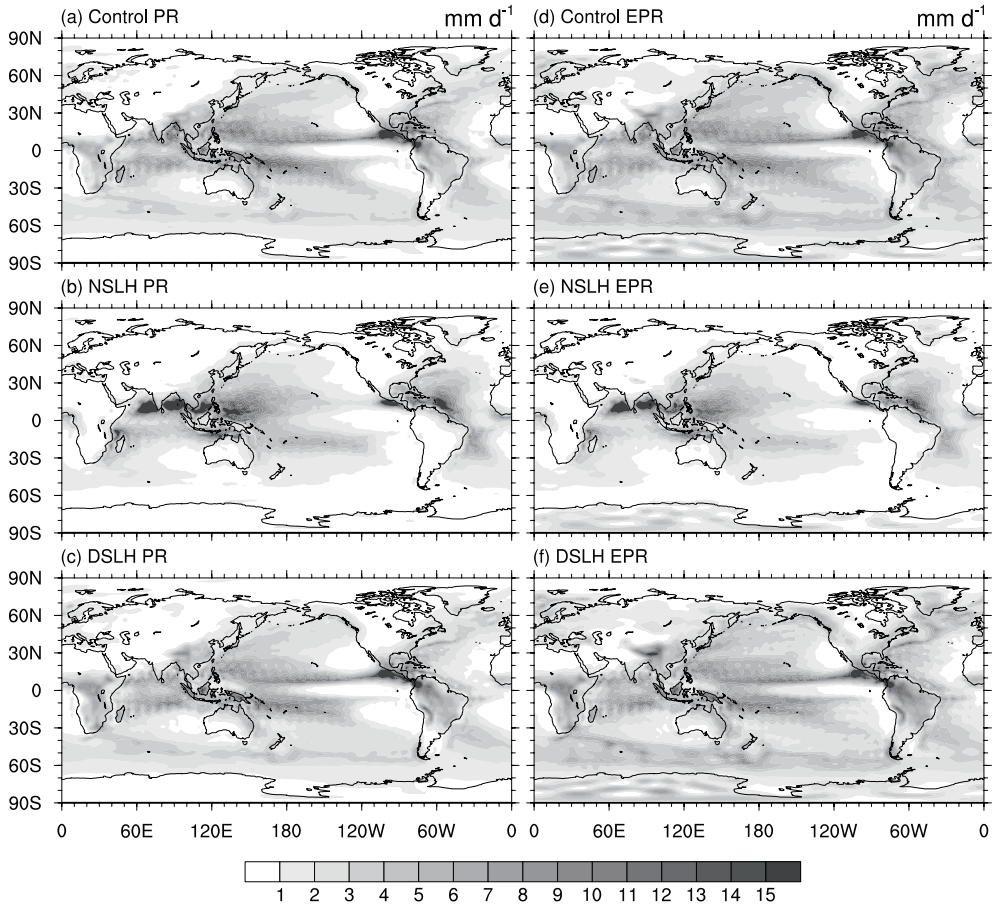

Fig. 4. (a–c) Mean precipitation (mm d^{-1}) and (d–f) EPR (mm d^{-1}) from the control run (top panel), the no shallow latent heating run (NSLH, middle), and the double shallow latent heating run (DSLH, bottom).

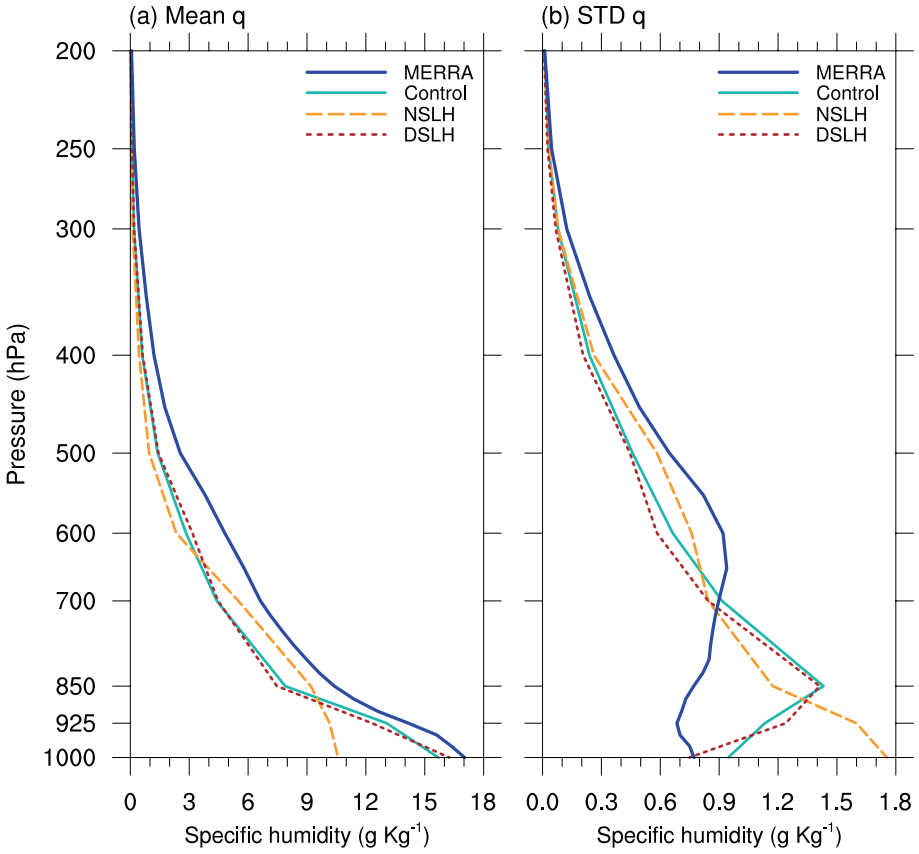

Fig. 5. Zonally averaged (a) mean and (b) standard deviations (g kg^{-1}) of specific humidity from 60°E to 180°E. All are total field and averaged over 15°S–15°N.

ern Hemisphere. There was no obvious change in precipitation in the DSLH run compared to the control run. Mean precipitation and EPR over the tropical region were almost the same in each of the three simulations. Large differences occurred only in high-latitude areas, especially Antarctica, where the precipitation was not dominated by the convection. Therefore, precipitation and latent heating were almost consistent in the mean state, and the amount of precipitation generated by shallow convection was small. The inconsistency between precipitation and latent heating due to model modifications did not have much influence on the other processes in the model. As previously mentioned, the shallow convection mostly occurred over the ocean (Fig. 3a). Once the precipitation was generated, it had only a weak influence on surface evaporation over the ocean. Therefore, precipitation was not diagnosed in this study.

Time mean moisture (q) profiles averaged over the region of strong observed MJO signals (15°S–15°N, 60°–180°E) from the three simulations were compared to results from MERRA (Fig. 5a). All three simulations suffered from dry biases. The moisture profiles from the control run and the DSLH run were almost identical, but the DSLH run was still somewhat drier than the control run below 700 hPa. The dry bias in the NSLH run was less than in the control run and the DSLH run in the lower troposphere but more severe below the 850 hPa level. This result may suggest that more moisture was transported from the PBL to the free atmosphere above it in the NSLH run than in the control run and the DSLH run.

3.2 *Total and intraseasonal variability*

The total variability of tropospheric moisture in the three simulations was evaluated (Fig. 5b). All failed to reproduce the results seen in the MERRA (solid blue line). The peak variability occurred at ~650 hPa in MERRA. A second, weaker peak occurred near the surface. The largest, and overestimated variability of moisture in the control run and the DSLH run occurred at a much lower level, near 850 hPa. The moisture variability in the NSLH run did not show any peak above the PBL but showed an overestimated peak near the surface. The large errors in the moisture variability in the lowest part of the atmosphere in the three simulations were related to unrealistic shallow precipitating cloud (and hence peaks in diabatic heat-

ing) within the PBL in the control run and the DSLH run and the surgical removal of the diabatic heating peak in the NSLH run. The moisture in the NSLH run had greater variability above the 700-hPa level when compared to the control run and the DSLH run. This result indicates that more moisture changes occurred at the mid troposphere in the NSLH run, that is, more deep convection occurred in the NSLH run.

In the control run (Fig. 6a) and the DSLH run (Fig. 6c), both total and intraseasonal variability of latent heating in the tropics were weaker compared to the NSLH run (Fig. 6b). The DSLH run had the weakest variability among the three SAMIL simulations. Figure 6 is consistent with Fig. 5b. The variability of moisture in the middle level and the latent heating were on the same order from weakest to strongest among these three simulations. We propose that enhanced latent heating peaks in the PBL in the control run and the DSLH run prevented the moisture in the PBL from being transported to the free atmosphere to provide a favorable environment for deep convection (Fig. 5a).

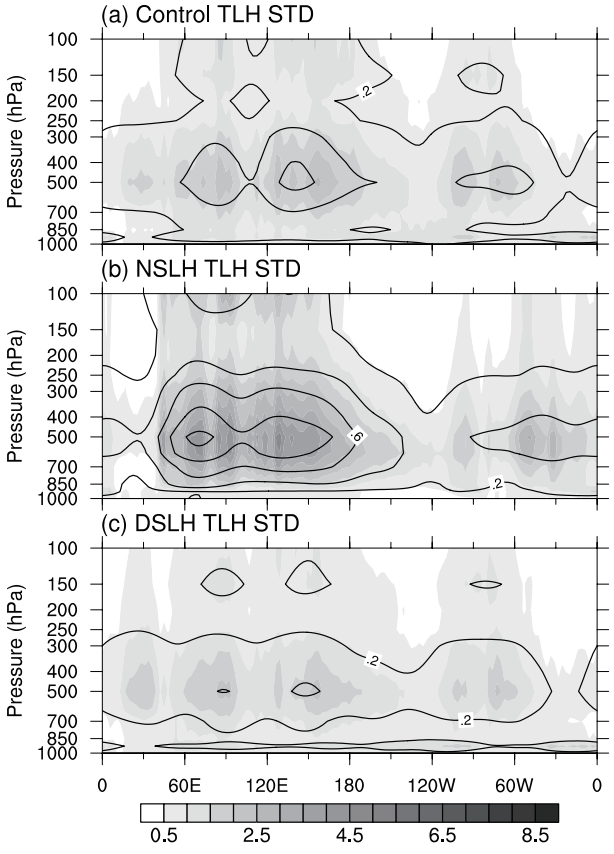

Fig. 6. Longitude–pressure distribution of total (shaded) and MJO band filtered (contour, interval 0.2) standard deviation of total latent heating (TLH, K d^{-1}) from (a) the control run, (b) the no shallow latent heating run (NSLH), and (c) the double shallow latent heating run (DSLH). All are averaged over 15°S–15°N.

3.3 *MJO signals*

Descriptions of observed characteristics of MJO, such as its space–time spectra, eastward propagation, and structure have been reported in many studies, and they were summarized by Lau and Waliser (2005) and Zhang (2005). They are not repeated here. The characteristic zonal scales, periods, and zonal propagation of the MJO can be diagnosed using time–space spectra (Hayashi, 1982). The time–space spectra of unfiltered zonal wind at 850 (U850) and 200 hPa (U200) and EPR from the three simulations are shown in Fig. 7. The spectra of U850 and U200 from the control run (Figs. 7a, b) showed power peaks in the intraseasonal band, but the eastward component was only slightly larger than its westward counterpart. There was no obvious intraseasonal peak in EPR (Fig. 7c). These results suggest that there was no strong eastward-propagating intraseasonal signal in the control run. The spectral characteristics of the DSLH run (Figs. 7g–i) was similar to the control run, but its intraseasonal power was even weaker. In contrast, the intraseasonal spectral peak of zonal wind from the NSLH run was well separated from lower and higher frequencies and its eastward component was obviously larger than its westward counterpart (Figs. 7d and e). However, the intraseasonal power maxima of the zonal wind occurred at period of 30–40 days, whereas its period was 53 days in the reanalysis (Fig. 3 of Zhang, 2005). This means that the intraseasonal signal in the zonal wind propagates faster than in observations, which is the common problem in most recent AGCMs (Zhang and Mu, 2005). The EPR spectrum for the NSLH run also showed greater power in the intraseasonal period, and it also had a larger wavenumber range (from 1 to 3) than those in the control run and the DSLH run. The NSLH run still had the problem in common with other MJO simulations in many other AGCMs: the intraseasonal large-scale circulation (zonal wind) and the convection (precipitation) were less coupled than in observations (Zhang et al., 2006).

Lag linear regression upon EPR at 90°E was applied to the MJO band-filtered U850 and the EPR of these three simulations. A confidence level of 90% was applied using the Student's t-test. The results (Fig. 8) confirmed what the spectra showed (Fig. 7). Neither U850 nor EPR from the control run or the DSLH run showed any eastward propagation. Weak westward propagation signals occurred in the EPR, related to the propagation of equatorial Rossby waves. U850 wind and EPR in the NSLH run both showed unques-

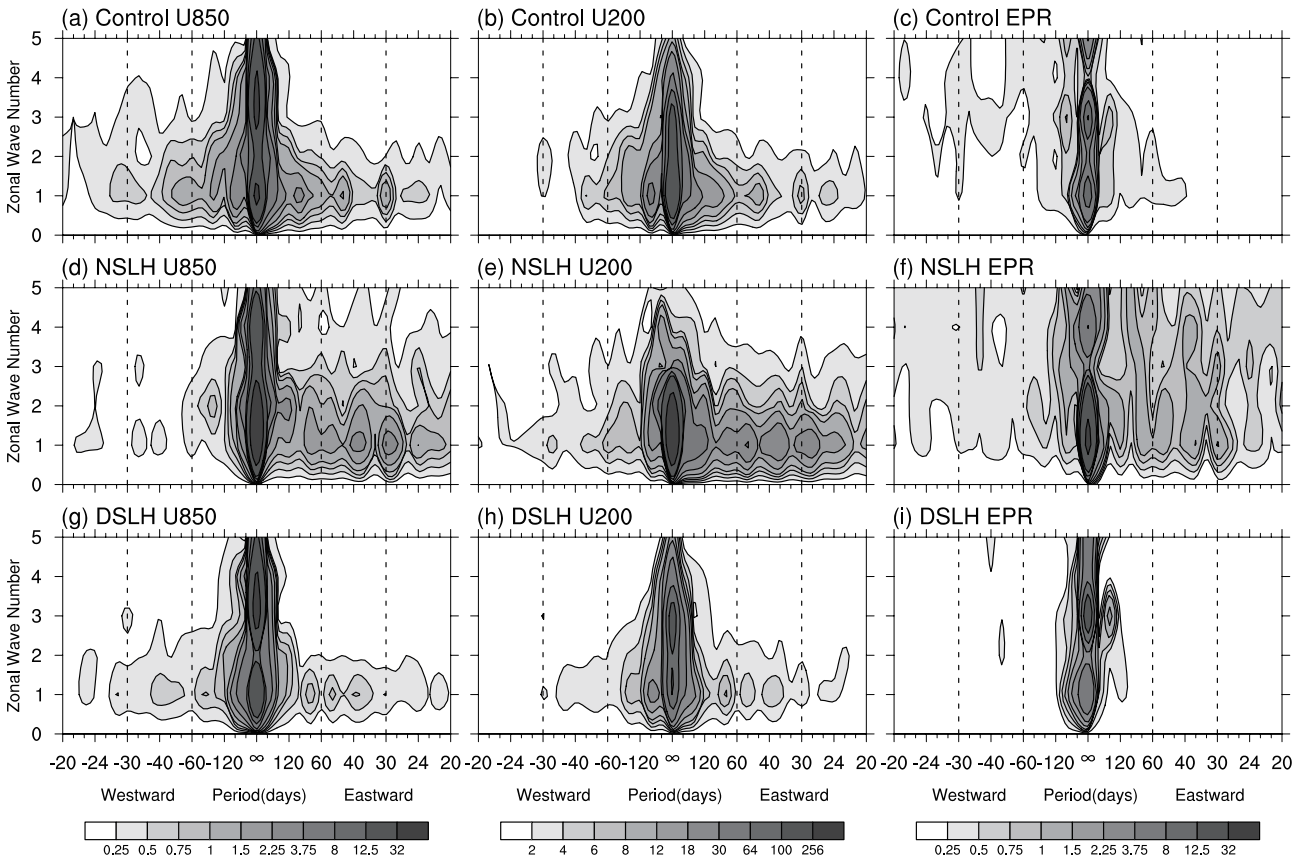

Fig. 7. Time–space spectra of U850 (left column), U200 (middle), and EPR (right) averaged from 15°S to 15°N from the control run (top panel), the no shallow latent heating run (NSLH, middle), and the double shallow latent heating run (DSLH, bottom) simulations. Amplitudes are scaled for best visual effects with different variables.

tionable eastward-propagating characteristics from the Indian Ocean to the western Pacific, with coherence speed close to (a little faster than) the observed MJO speed (5 m s^{-1}). According to these diagnostic results, only the NSLH run produced the MJO signal among these three simulations.

3.4 *Moisture convergence*

The larger latent heating peak in the PBL in the DSLH run confined more moisture to the PBL, and less deep convection was generated when compared to the control run. Therefore, the intraseasonal variability in the DSLH run was very similar to that in the control run, except the amplitude was smaller (Figs. 6–8). Only the results from the control run and the NSLH run simulations were further compared.

The vertical profiles of the moisture tendency for each term from Eq. (3) in section 2.3 were averaged over the region where MJO exists (15°S–15°N, 60°–180°E) are shown in Fig. 9. The large-scale horizontal circulation converged moisture in the low atmosphere, and the larger-scale vertical motion moved the moisture to higher levels in the troposphere. The horizontal moisture convergence extended up to 700 hPa in the NSLH run and only to 850 hPa in the control run. Furthermore, the large-scale vertical motion pumped moisture to a much higher level in the NSLH run than in the control run. Therefore, the large-scale circulation was more efficient at moistening the low and mid troposphere in the NSLH run than in the control run, which led to more generation of deep convection.

The vertical convergence of vertical eddy transport of moisture transport, estimated as a residual from the moisture budget equation (Eq. 3), is also shown in Fig. 9c. This term depicts the sub-grid processes that play an important role in convection. Convection in the NSLH run pumped more moisture into the free atmosphere, while more moisture was confined to the PBL, and less was transported to the free atmosphere in the control run. Therefore, there was a dry bias in the control run within the free atmosphere compared to the NSLH run, which led to a shorter lifetime of deep convection. Not only the large-scale circulation but also the vertical eddy transport were more efficient

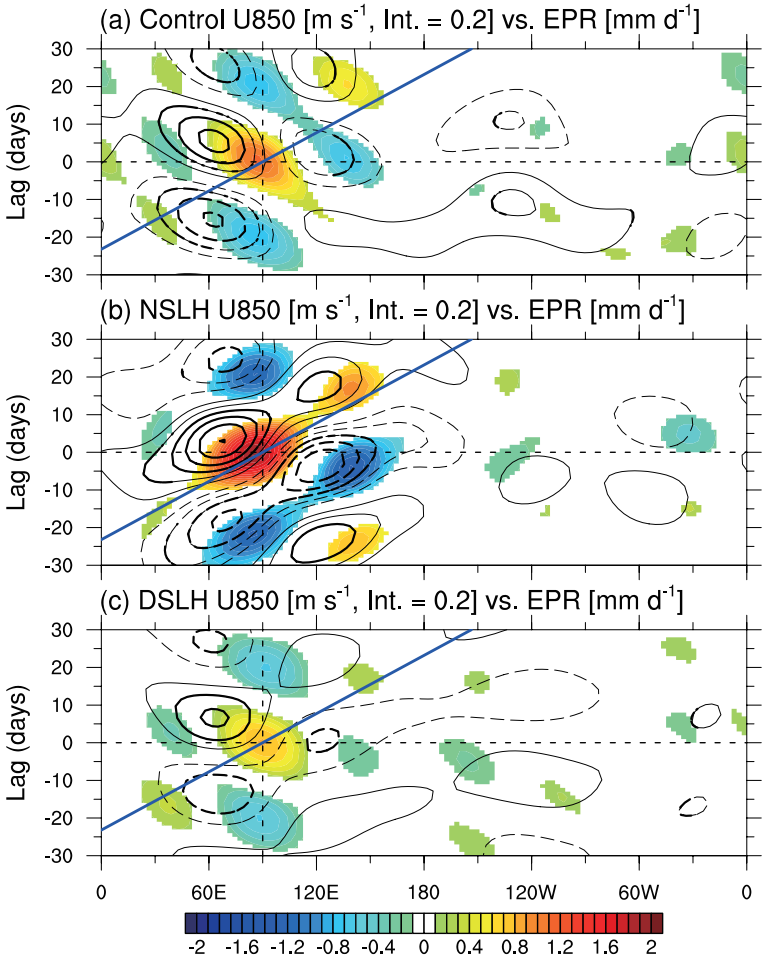

Fig. 8. Lag regression of MJO band filtered U850 (contour, interval 0.2 m s^{-1}) and EPR (shaded, mm d^{-1}) upon EPR at 90°E (0 day) from (a) the control run, (b) the no shallow latent heating run (NSLH), and (c) the double shallow latent heating run (DSLH). All the data were first averaged over 15°S–15°N. Dashed contours for negative values and zero contours were omitted. Only results passing a significant test with the 90% confidence level or above were plotted for EPR, highlighted by thick contours for U850. The blue thick solid lines represent the 5 m s^{-1} eastward propagation speed.

at transporting moisture to the free atmosphere in the NSLH run than in the control run. The largest vertical velocity was almost in phase with the largest latent heating in the tropical region. Therefore, moisture convergence due to the large-scale vertical motion and vertical eddy transport was also in phase with heating. It therefore was not able to influence the propagating direction of the convection center, but it did influence the lifetime of the convection.

Structures of latent heating and large-scale horizontal moisture convergence in the control run and the NSLH run along with their associated zonal-vertical circulations are shown in Fig. 10. If either the zonal wind or the vertical velocity passed the significance test (confidence level: 90%), the wind vector was drawn. Strong zonal and vertical circulation occurred in the NSLH run, and the zonal wind was of a typical deep, first baraclinic mode extending from the surface up to 150 hPa, with mid-level upward motion, low-level convergence, and upper-level divergence in regions of positive moisture, and mid-level downward motion, low-level divergence, and upper-level convergence in regions of negative moisture. The manifestation of the MJO in latent heating and its associated circulation was not obvious in the control run. Latent heating and its associated vertical zonal motion were much weaker and shallower than in the NSLH run.

Lower level moisture convergence was weak, shal-

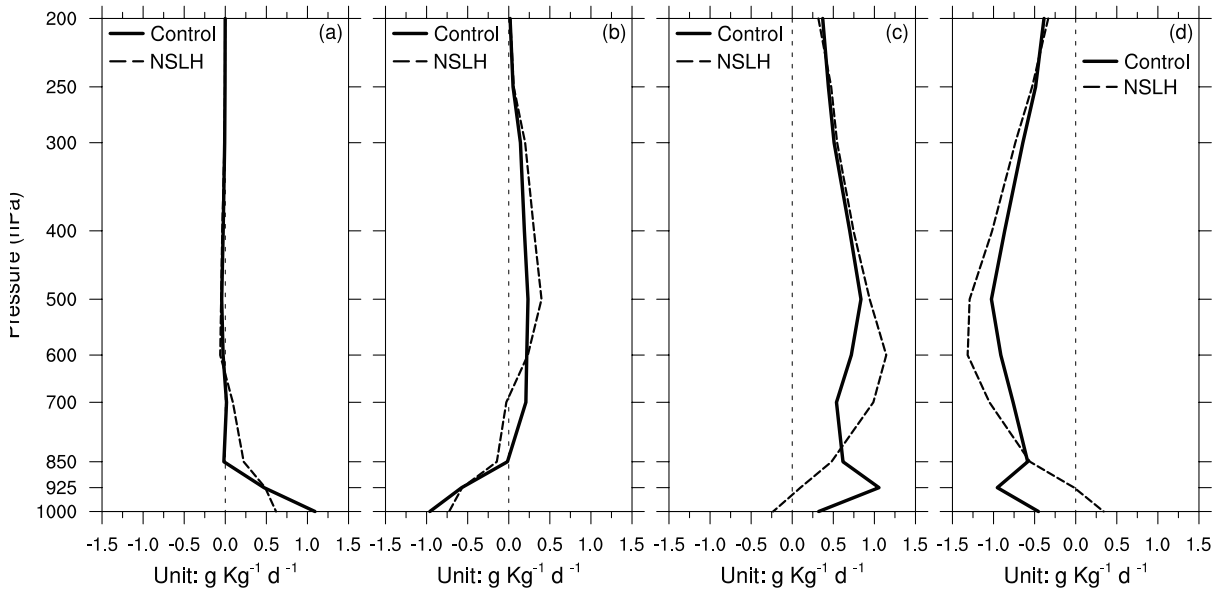

Fig. 9. The vertical profiles of moisture convergence (g kg^{-1} d^{-1}) from the larger scale (a) horizontal and (b) vertical convergence, (c) vertical eddy transport, and (d) precipitation and evaporation. All was averaged over 60°–180°E and 15°S–15°N.

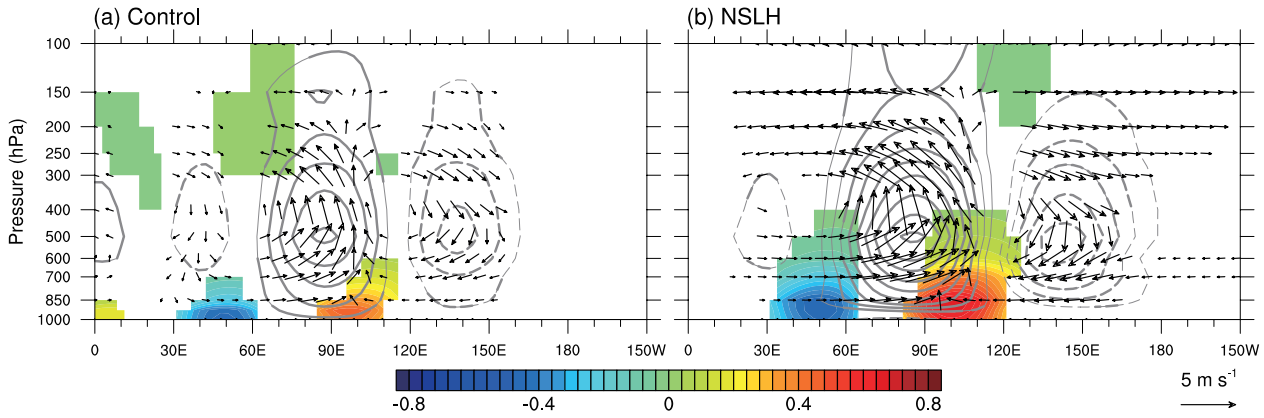

Fig. 10. Longitude–pressure distributions of tropical averaged (15°S–15°N) latent heating (contour, interval 0.1 K d^{-1}), moisture convergence (color, 10^{-5} g kg^{-1} s^{-1}) and zonal-vertical wind vectors of the MJO regressed upon MJO EPR at 90°E with time lag 0 day from (a) the control run, and (b) the no shallow latent heating run (NSLH). Dashed contours for negative values and zero contours omitted. Only results passing a significant test with the 90% confidence level or above are plotted for moisture convergence and zonal-vertical wind, highlighted by thick contours for latent heating.

low, and small in its zonal scale in the control run, while the low-level moisture convergence became stronger and deeper, and its zonal scales were larger in the NSLH run. The strong low-level moisture convergence that reached up to 500 hPa was located east of the latent heating center in the NSLH run, which provided plenty of moisture to the east of the existing convection center and set the stage for the generation of deep convection there. This result is consistent with the MJO theory in terms of boundary layer frictional convergence (Wang, 1988; Wang and Rui, 1990), and this might be the reason for the eastward propagation of simulated MJO in the NSLH run. The difference between the low-level moisture convergence in these two simulations was caused by shallow convection that resulted from using the Tiedtke scheme, which generated the PBL latent-heating peak. This peak tended to confine the moisture to the PBL and prevented it from being transported to the free atmosphere, not only by the larger-scale circulation (Figs. 9a and b) but

also by the vertical eddy transport (Fig. 9c). This result is consistent with previous studies. Tiedtke (1989) showed that the cloud layer below the PBL becomes moister when the latent heating peak in the PBL increases.

4. Summary and discussion

In this study, the role of a latent heating peak in the PBL in MJO simulations by an AGCM was investigated. This AGCM failed to produce the MJO in its control run simulation. Two sensitivity experiments were designed to explore the reason for its failure.

When latent heating in the PBL was artificially removed (the NSLH run), reasonable MJO signals were produced. When the latent heating peak in the PBL was enhanced (the DSLH run), the variability of zonal wind and latent heating all became even weaker than in the control run in both their total and intraseasonal components. The latent heating peak in the PBL prevented moisture from being transported to the free atmosphere from the PBL not only by the large-scale motion but also by the subgrid-scale processes. Even if deep convection still pumped moisture from the PBL into the troposphere, without a favorable moist lower troposphere this process was localized and short lived (Fig. 9c). When the latent heating peak in the PBL was removed in the NSLH run, more moisture evaporated from the sea surface was transported to the free atmosphere, which provided a favorable environment for the deep convection to develop and eventually led to MJO in the simulation.

Previous numerical studies have clearly demonstrated the dependence of tropical deep convection on tropospheric moisture (Tompkins, 2001; Derbyshire et al., 2004), especially the moisture variations in the lower troposphere above the cloud base (Sherwood and Wahrlich, 1999; Sobel et al., 2004; Holloway and Neelin, 2009). Increasing low-level moisture leading to active phases of the MJO has been shown in many studies using observations/reanalysis data (Johnson et al., 1999; Kemball-Cook et al., 2002; Kiladis et al., 2005), and simulations by climate models (Thayer-Calder and Randall, 2009; Zhang and Song, 2009) and weather prediction models (Agudelo et al., 2009). Hagos et al. (2011) found that the failure of the cumulus parameterization to provide the adequate low-level moistening was the reason for poor MJO simulation of the TWRF.

The results from this study confirm the critical role of vertical moisture distribution in MJO simulations, but they offer a new perspective. It has been commonly assumed that shallow convection and convective conjectures may be crucial to low-level moistening needed for the MJO (Johnson et al., 1999). This moistening role played by shallow convection was constructed in a recent MJO theory (Majda and Stechmann, 2009); Woolnough et al. (2010) also found that in a cloud-resolving mode, predominant shallow convection in suppressed phases of MJO led to maximum moistening in the free atmosphere (around 3 km). However, the top of convection identified as shallow convection in the Tiedtke scheme in the SAMIL model did not reach 700 hPa (see section 2.2), so the lower-tropopshere was not moistened by these boundary-layer shallow clouds in our simulations. The latent-heating profiles indicate that these shallow clouds precipitated in our models. The problem is that they precipitated too much and erroneously weakened the large-scale circulation. They therefore acted as a "moisture barrier" to prevent moisture from being transported into the lower troposphere. This led to a dry bias in the free atmosphere, which did not allow the MJO to occur in the control simulation. We thus conclude that, while precipitating shallow convection might be needed for the MJO, too much precipitating shallow convection in the PBL was detrimental to MJO simulations. However, it is difficult to determine how much is too much, due to the limitations of in situ observations.

The brute force method used in this study to remove boundary layer latent heating may have created negative consequences. For example, the model mean state (e.g., precipitation, air temperature) was degraded. Tuning model parameterizations for better MJO simulations often degrades the mean climate of the model (Sobel et al., 2010). The sensitivity simulations in this study were meant only to demonstrate the causes of the poor or no MJO reproduction in the SAMIL model. They might be causes for similar problems in other models. For a complete understanding of the role of latent heating in MJO simulations, we need to design better and more complex numerical experiments without breaking consistency among different variables and energy conservation, so the model climatology is not affected too much. Accurate observations of latent heating profiles, especially in the lowest part of the atmosphere, are also needed to validate numerical experiments.

Acknowledgements. Part of this study was done during the first author's Ph. D studies at the Institute of Atmospheric Physics in China. Two anonymous reviewers provided constructive comments to an early manuscript of this study. The authors thank Marcela Ulate Medrano for providing the WRF latent heating data. This study was supported by National Science Foundation of U.S.A. (Grant No. ATM0739402) and the National Natural Sci-

ence Foundation of China (Grant Nos. U0833602 and 40905035).

REFERENCES

Agudelo, P. A., C. D. Hoyos, P. J. Webster, and J. A. Curry, 2009: Application of a serial extended forecast experiment using the ECMWF model to interpret the predictive skill of tropical intraseasonal variability. *Climate Dyn.*, **32**, 855–872.

Benedict, J. J., and D. A. Randall, 2007: Observed characteristics of the MJO relative to maximum rainfall. *J. Atmos. Sci.*, **64**, 2332–2354.

Bosilovich, M., S. Schubert, G. Kim, R. Gelaro, M. Rienecker, M. Suarez, and R. Todling, 2006: NASA' s Modern Era Retrospective-analysis for Research and Applications (MERRA). *US CLIVAR Variations*, **4**, 5–8.

Chang, C. P., and H. Lim, 1988: Kelvin wave-CISK: A possible mechanism for the 30–50 day oscillations. *J. Atmos. Sci.*, **45**, 1709–1720.

Cho, H. R., and D. Pendlebury, 1997: Wave CISK of equatorial waves and the vertical distribution of cumulus heating. *J. Atmos. Sci.*, **54**, 2429–2440.

Derbyshire, S. H., I. Beau, P. Bechtold, J. Y. Grandpeix, J. M. Piriou, J. L. Redelsperger, and P. M. M. Soares, 2004: Sensitivity of moist convection to environmental humidity. *Quart. J. Roy. Meteor. Soc.*, **130**, 3055–3079.

Edwards, J. M., and A. Slingo, 1996: Studies with a flexible new radiation code. I: Choosing a configuration for a large-scale model. *Quart. J. Roy. Meteor. Soc.*, **122**, 689–719.

Fu, X. H., and B. Wang, 2009: Critical roles of the stratiform rainfall in sustaining the Madden–Julian Oscillation: GCM experiments. *J. Climate*, **22**, 3939–3959.

Gregory, D., R. Kershaw, and P. M. Inness, 1997: Parametrization of momentum transport by convection. II: Tests in single-column and general circulation models. *Quart. J. Roy. Meteor. Soc.*, **123**, 1153–1183.

Hagos, S., L. R. Leung, and J. Dudhia, 2011: Thermodynamics of Madden–Julian Oscillation in a regional model with constrained moisture. *J. Atmos. Sci.*, **68**, 1974–1989.

Hartmann, D. L., H. H. Hendon, and R. A. Houze, 1984: Some implications of the mesoscale circulations in tropical cloud clusters for large-scale dynamics and climate. *J. Atmos. Sci.*, **41**, 113–121.

Hayashi, Y., 1982: Space–time spectral analysis and its applications to atmospheric waves. *J. Meteor. Soc. Japan*, **60**, 156–171.

Holloway, C. E., and J. D. Neelin, 2009: Moisture vertical structure, column water vapor, and tropical deep convection. *J. Atmos. Sci.*, **66**, 1665–1683.

Holtslag, A. A. M., and B. A. Boville, 1993: Local versus nonlocal boundary-layer diffusion in a global climate model. *J. Climate*, **6**, 1825–1842.

Houze, R. A., 1997: Stratiform precipitation in regions of convection: A meteorological paradox? *Bull. Amer. Meteor. Soc.*, **78**, 2179–2196.

Inness, P. M., and D. Gregory, 1997: Aspects of the intraseasonal oscillation simulated by the Hadley Centre Atmosphere Model. *Climate Dyn.*, **13**, 441–458.

Jia, X. L., C. Y. Li, J. Ling, and C. D. Zhang, 2008: Impacts of a GCM's resolution on MJO simulation. *Adv. Atmos. Sci.*, **25**, 139–156, doi: 10.1007/s00376-008-0319-9.

Jia, X. L., C. Y. Li, N. F. Zhou, and J. Ling, 2010: The MJO in an AGCM with three different cumulus parameterization schemes. *Dyn. Atmos. Oceans*, **49**, 141–163.

Johnson, R. H., T. M. Rickenbach, S. A. Rutledge, P. E. Ciesielski, and W. H. Schubert, 1999: Trimodal characteristics of tropical convection. *J. Climate*, **12**, 2397–2418.

Kalnay, E., and Coauthors, 1996: The NCEP/NCAR 40-year reanalysis project. *Bull. Amer. Meteor. Soc.*, **77**, 437–471.

Katsumata, M., R. H. Johnson, and P. E. Ciesielski, 2009: Observed synoptic-scale variability during the developing phase of an ISO over the Indian Ocean during MISMO. *J. Atmos. Sci.*, **66**, 3434–3448.

Kemball-Cook, S., B. Wang, and X. H. Fu, 2002: Simulation of the intraseasonal oscillation in the ECHAM-4 model: The impact of coupling with an ocean model. *J. Atmos. Sci.*, **59**, 1433–1453.

Kiladis, G. N., K. H. Straub, and P. T. Haertel, 2005: Zonal and vertical structure of the Madden–Julian oscillation. *J. Atmos. Sci.*, **62**, 2790–2809.

Kiladis, G. N., M. C. Wheeler, P. T. Haertel, K. H. Straub, and P. E. Roundy, 2009: Convectively coupled equatorial waves. *Rev. Geophys.*, **47**, doi: 10.1029/2008RG000266.

Kim, D., and Coauthors, 2009: Application of MJO simulation diagnostics to climate Models. *J. Climate*, **22**, 6413–6436.

Lau, K. M., and L. Peng, 1987: Origin of low-frequency (intraseasonal) oscillations in the tropical atmosphere. I. Basic theory. *J. Atmos. Sci.*, **44**, 950–972.

Lau, K. M., and D. E. Waliser, 2005: *Intraseasonal Variability in the Atmosphere–Ocean Climate System.* Springer, 436pp.

Lee, M. I., I. S. Kang, and B. E. Mapes, 2003: Impacts of cumulus convection parameterization on aqua-planet AGCM Simulations of tropical intraseasonal variability. *J. Meteor. Soc. Japan*, **81**, 963–992.

Li, C., 1985: Actions of summer monsoon troughs (ridges) and tropical cyclone over South Asia and the moving CISK mode. *Scientia Sinica* (*B*), **28**, 1197–1206.

Li, C. Y., X. L. Jia, J. Ling, W. Zhou, and C. D. Zhang, 2009: Sensitivity of MJO simulations to diabatic heating profiles. *Climate Dyn.*, **32**, 167–187.

Lin, J. L., B. Mapes, M. H. Zhang, and M. Newman, 2004: Stratiform precipitation, vertical heating profiles, and the Madden-Julian Oscillation. *J. Atmos.*

Sci., **61**, 296–309.

Lin, J. L., and Coauthors, 2006: Tropical intraseasonal variability in 14 IPCC AR4 climate models. Part I: Convective signals. *J. Climate*, **19**, 2665–2690.

Ling, J., and C. D. Zhang, 2011: Structural evolution in heating profiles of the MJO in global reanalyses and TRMM retrievals. *J. Climate*, **24**, 825–842.

Ling, J., and C. D. Zhang, 2012: Diabatic heating profiles in recent global reanalyses. *J. Climate*, doi: 10.1175/JCLI-D-12-00384.1. (in press)

Ling, J., C. Y. Li, and X. L. Jia, 2009: Impacts of Cumulus momentum transport on MJO simulation. *Adv. Atmos. Sci.*, **26**, 864–876, doi: 10.1007/s00376-009-8016-8.

Liu, P., B. Wang, K. R. Sperber, T. Li, and G. A. Meehl, 2005: MJO in the NCAR CAM2 with the Tiedtke convective scheme. *J. Climate*, **18**, 3007–3020.

Madden, R. A., and P. R. Julian, 1971: Detection of a 40–50 day oscillation in zonal wind in tropical Pacific. *J. Atmos. Sci.*, **28**, 702–708.

Madden, R. A., and P. R. Julian, 1972: Description of global-scale circulation cells in tropics with a 40–50 day period. *J. Atmos. Sci.*, **29**, 1109–1123.

Madden, R. A., and P. R. Julian, 1994: Observations of the 40–50-day tropical oscillation—A review. *Mon. Wea. Rev.*, **122**, 814–837.

Majda, A. J., and S. N. Stechmann, 2009: The skeleton of tropical intraseasonal oscillations. *Proc. Natl. Acad. Sci. USA*, **106**, 8417–8422.

Maloney, E. D., and D. L. Hartmann, 2001: The sensitivity of intraseasonal variability in the NCAR CCM3 to changes in convective parameterization. *J. Climate*, **14**, 2015–2034.

Manabe, S., and R. F. Strickler, 1964: Thermal equilibrium of the atmosphere with a convective adjustment. *J. Atmos. Sci.*, **21**, 361–385.

Mapes, B. E., 2000: Convective inhibition, subgrid-scale triggering energy, and stratiform instability in a toy tropical wave model. *J. Atmos. Sci.*, **57**, 1515–1535.

Nordeng, T. E., 1994: Extended versions of the convective parameterization scheme at ECMWF and their impact on the mean and transient activity of the model in the tropics. Tech. Memo. No. 206, ECMWF, Reading, England, 41pp.

Rajendran, K., R. S. Nanjundiah, and J. Srinivasan, 2002: Comparison of seasonal and intraseasonal variation of tropical climate in NCAR CCM2 GCM with two different cumulus schemes. *Meteor. Atmos. Phys.*, **79**, 57–86.

Saha, S., and Coauthors, 2010: The NCEP climate forecast system reanalysis. *Bull. Amer. Meteor. Soc.*, **91**, 1015–1057.

Schumacher, C., R. A. Houze, and I. Kraucunas, 2004: The tropical dynamical response to latent heating estimates derived from the TRMM precipitation radar. *J. Atmos. Sci.*, **61**, 1341–1358.

Sherwood, S. C., and R. Wahrlich, 1999: Observed evolution of tropical deep convective events and their environment. *Mon. Wea. Rev.*, **127**, 1777–1795.

Simmonds, I., 1985: Analysis of the "Spinup" of a general-circulation model. *J. Geophys. Res.*. **90**, 5637–5660.

Slingo, J. M., 1980: A cloud parametrization scheme derived from gate data for use with a numerical model. *Quart. J. Roy. Meteor. Soc.*, **106**, 747–770.

Slingo, J. M., 1987: The development and verification of a cloud prediction scheme for the ECMWF model. *Quart. J. Roy. Meteor. Soc.*, **113**, 899–927.

Slingo, J. M., and Coauthors, 1996: Intraseasonal oscillations in 15 atmospheric general circulation models: Results from an AMIP diagnostic subproject. *Climate Dyn.*, **12**, 325–357.

Sobel, A., E. Maloney, G. Bellon, and D. Frierson, 2010: Surface fluxes and tropical intraseasonal variability: A reassessment. *Journal of Advances in Modeling Earth Systems*, **2**(2), doi: 10.3894/JAMES.2010.2.2.

Sobel, A. H., S. E. Yuter, C. S. Bretherton, and G. N. Kiladis, 2004: Large-scale meteorology and deep convection during TRMM KWAJEX. *Mon. Wea. Rev.*, **132**, 422–444.

Song, X. L., 2005: The evaluation analysis of two kinds of mass-flux cumulus parameterization in climate simulation. Ph. D. dissertation, Institute of Atmospheric Physics, Chinese Academy of Sciences, 158pp. (in Chinese)

Sui, C. H., and K. M. Lau, 1989: Origin of low-frequency (intraseasonal) oscillations in the tropical atmosphere. 2. Structure and propagation of mobile wave-CISK modes and their modification by lower boundary forcings. *J. Atmos. Sci.*, **46**, 37–56.

Takahashi, M., 1987: A theory of the slow phase speed of the intraseasonal oscillation using the wave-Cisk. *J. Meteor. Soc. Japan*, **65**, 43–49.

Thayer-Calder, K., and D. A. Randall, 2009: The role of convective moistening in the Madden–Julian Oscillation. *J. Atmos. Sci.*, **66**, 3297–3312.

Tiedtke, M., 1989: A comprehensive mass flux scheme for cumulus parameterization in large-scale models. *Mon. Wea. Rev.*, **117**, 1779–1800.

Tompkins, A. M., 2001: Organization of tropical convection in low vertical wind shears: The role of water vapor. *J. Atmos. Sci.*, **58**, 529–545.

Wang, B., 1988: Dynamics of tropical low frequency waves: An analysis of the moist Kelvin wave. *J. Atmos. Sci.*, **45**, 2051–2065.

Wang, B., 2005: Theories. *Intraseasonal Variability in the Atmosphere-Ocean Climate System*, K. M. Lau and D. E. Waliser, Eds., Springer-Verlag, 436pp.

Wang, B., and H. Rui, 1990: Synoptic climatology of transient tropical intraseasonal convection anomalies—1975–1985. *Meteor. Atmos. Phys.*, **44**, 43–61.

Wang, W. Q., and M. E. Schlesinger, 1999: The dependence on convection parameterization of the tropical intraseasonal oscillation simulated by the UIUC 11-layer atmospheric GCM. *J. Climate*, **12**, 1423–1457.

Wang, X., D. X. Wang, W. Zhou, and C. Y. Li, 2012: Interdecadal modulation of the influence of

La Niña events on mei-yu rainfall over the Yangtze River valley. *Adv. Atmos. Sci.*, **29**, 157–168, doi: 10.1007/s00376-011-1021-8.

Webster, P., and R. Lukas, 1992: TOGA COARE: The coupled ocean–atmosphere response experiment. *Bull. Amer. Meteor. Soc.*, **73**, 1377–1416.

Woolnough, S. J., and Coauthors, 2010: Modelling convective processes during the suppressed phase of a Madden-Julian oscillation: Comparing single-column models with cloud-resolving models. *Quart. J. Roy. Meteor. Soc.*, **136**, 333–353.

Wu, G., L. Hui, Z. Yucheng, and L. Weiping, 1996: A nine-layer atmospheric general circulation model and its performance. *Adv. Atmos. Sci.*, **13**, 1–18.

Yanai, M., S. Esbensen, and J. H. Chu, 1973: Determination of bulk properties of tropical cloud clusters from large-scale heat and moisture budgets. *J. Atmos. Sci.*, **30**, 611–627.

Zhang, C. D., 2005: Madden-Julian Oscillation. *Rev. Geophys.*, **43**, RG2003, doi: 10.1029/2004RG000158.

Zhang, C. D., and S. M. Hagos, 2009: Bi-modal structure and variability of large-scale diabatic heating in the Tropics. *J. Atmos. Sci.*, **66**, 3621–3640.

Zhang, C. D., M. Dong, S. Gualdi, H. H. Hendon, E. D. Maloney, A. Marshall, K. R. Sperber, and W. Q. Wang, 2006: Simulations of the Madden–Julian Oscillation in four pairs of coupled and uncoupled global models. *Climate Dyn.*, **27**, 573–592.

Zhang, C. D., and Coauthors, 2010: MJO signals in latent heating: Results from TRMM retrievals. *J. Atmos. Sci.*, **67**, 3488–3508.

Zhang, G. J., and N. A. McFarlane, 1995: Sensitivity of climate simulations to the parameterization of cumulus convection in the Canadian Climate Center general-circulation model. *Atmos.–Ocean*, **33**, 407–446.

Zhang, G. J., and M. Q. Mu, 2005: Simulation of the Madden-Julian Oscillation in the NCAR CCM3 using a revised Zhang–McFarlane convection parameterization scheme. *J. Climate*, **18**, 4046–4064.

Zhang, G. J., and X. L. Song, 2009: Interaction of deep and shallow convection is key to Madden–Julian Oscillation simulation. *Geophys. Res. Lett.*, **36**, L09708, doi: 10.1029/2009GL037340.